Kidney360

Clinical Relevance of Computationally Derived Attributes of Peritubular Capillaries from Kidney Biopsies

Yijiang Chen,[1] Jarcy Zee,[2,3] Andrew R. Janowczyk,[4,5] Jeremy Rubin,[2] Paula Toro,[6] Kyle J. Lafata,[7,8,9] Laura H. Mariani,[10] Lawrence B. Holzman,[11] Jeffrey B. Hodgin,[12] Anant Madabhushi,[13,5] and Laura Barisoni[14,15]

Key Points

- Computational image analysis allows for the extraction of new information from whole-slide images with potential clinical relevance.
- Peritubular capillary (PTC) density is decreased in areas of interstitial fibrosis and tubular atrophy when measured in interstitial fractional space.
- PTC shape (aspect ratio) is associated with clinical outcome in glomerular diseases.

Abstract

Background The association between peritubular capillary (PTC) density and disease progression has been studied in a variety of kidney diseases using immunohistochemistry. However, other PTC attributes, such as PTC shape, have not been explored yet. The recent development of computer vision techniques provides the opportunity for the quantification of PTC attributes using conventional stains and whole-slide images.

Methods To explore the relationship between PTC characteristics and clinical outcome, n=280 periodic acid–Schiff-stained kidney biopsies (88 minimal change disease, 109 focal segmental glomerulosclerosis, 46 membranous nephropathy, and 37 IgA nephropathy) from the Nephrotic Syndrome Study Network digital pathology repository were computationally analyzed. A previously validated deep learning model was applied to segment cortical PTCs. Average PTC aspect ratio (PTC major to minor axis ratio), size (PTC pixels per PTC segmentation), and density (PTC pixels per unit cortical area) were computed for each biopsy. Cox proportional hazards models were used to assess associations between these PTC parameters and outcome (40% eGFR decline or kidney failure). Cortical PTC characteristics and interstitial fractional space PTC density were compared between areas of interstitial fibrosis and tubular atrophy (IFTA) and areas without IFTA.

Results When normalized PTC aspect ratio was below 0.6, a 0.1, increase in normalized PTC aspect ratio was significantly associated with disease progression, with a hazard ratio (95% confidence interval) of 1.28 (1.04 to 1.59) (P = 0.019), while PTC density and size were not significantly associated with outcome. Interstitial fractional space PTC density was lower in areas of IFTA compared with non-IFTA areas.

Conclusions Computational image analysis enables quantification of the status of the kidney microvasculature and the discovery of a previously unrecognized PTC biomarker (aspect ratio) of clinical outcome.

KIDNEY360 4: 648–658, 2023. doi: https://doi.org/10.34067/KID.0000000000000116

[1]Center for Computational Imaging and Personalized Diagnostics, Case Western Reserve University, Cleveland, Ohio
[2]Department of Biostatistics, Epidemiology, and Informatics, University of Pennsylvania, Philadelphia, Pennsylvania
[3]Children's Hospital of Philadelphia, Philadelphia, Pennsylvania
[4]Geneva University Hospitals, Pathology and Oncology Departments, Geneva, Switzerland
[5]Department of Biomedical Engineering, Emory University and Georgia Institute of Technology, Atlanta, Georgia
[6]Department of Pathology, Cleveland Clinic, Cleveland, Ohio
[7]Department of Radiology, Duke University, Durham, North Carolina
[8]Department of Electrical and Computer Engineering, Duke University, Durham, North Carolina
[9]Department of Radiation Oncology, Duke University, Durham, North Carolina
[10]Department of Internal Medicine, Division of Nephrology, University of Michigan, Ann Arbor, Michigan
[11]Department of Medicine, Renal-Electrolyte and Hypertension Division, University of Pennsylvania, Philadelphia, Pennsylvania
[12]Department of Pathology, University of Michigan, Ann Arbor, Michigan
[13]Atlanta Veterans Affairs Medical Center, Atlanta, Georgia
[14]Department of Pathology, Division of AI and Computational Pathology, Duke University, Durham, North Carolina
[15]Department of Medicine, Division of Nephrology, Duke University, Durham, North Carolina

Correspondence: Dr. Laura Barisoni, Department of Pathology, Division of AI and Computational Pathology, and Department of Medicine, Division of Nephrology, Duke University. 40 Medicine Circle, Durham NC, 27710, or Dr. Anant Madabhushi, Atlanta Veterans Administration Medical Center, Wallace H. Coulter Department of Biomedical Engineering, Radiology and Imaging Sciences, Biomedical Informatics (BMI) and Pathology, Georgia Institute of Technology, Emory University, Health Sciences Research Building, 1750 Haygood Drive II, Suite W212, Atlanta, GA 30322. E-mail: laura.barisoni@duke.edu or anantm@emory.edu

Introduction

Morphologic assessment of kidney biopsies remains the gold standard for diagnosis of renal diseases.[1] In glomerular diseases, current diagnostic approaches are based on visual assessment of the renal cortex, with notable attention paid to the glomerular compartment.[2] Recent studies have shown that assessment of tubulointerstitial and vascular compartments provide additional information that can ameliorate outcome prediction and biomarker discovery for improved clinical care.[3–5] However, the status of the kidney microvasculature, mostly composed of peritubular capillaries (PTCs), has not yet been fully explored. Critically, PTC morphologic characteristics may have an undiscovered role in modulating perfusion and oxygenation of kidney tissue contributing to the progression of tubulointerstitial changes and ultimately resulting in poor outcome.[6–10]

With the advent of digital pathology and development of computerized pathology image analysis, there is an unprecedented opportunity to automatically segment PTCs[11] and precisely and deterministically extract and quantify a variety of characteristics from these PTCs.[12] The computational measurements of PTC characteristics may not only increase accuracy and reproducibility of observations compared with visual assessment but also offer the opportunity for discovery of novel prognostic image biomarkers.

In this study, we applied computational image analysis tools on the Nephrotic Syndrome Study Network (NEPTUNE) digital kidney biopsies[13] to explore whether characteristics of segmented PTCs, such as density, size, and shape, may serve as biomarkers of progression in glomerular diseases.

Materials and Methods

Study Sample Selection

The current study leveraged the infrastructure of the NEPTUNE consortium, a multisite observational cohort study of children and adults with proteinuria, enrolled at the time of their first clinically indicated kidney biopsy.[13] NEPTUNE participants with (*1*) a digital renal biopsy and a periodic acid–Schiff (PAS)-stained whole-slide image (WSI) stored in the NEPTUNE digital pathology repository that passed quality control (see WSI quality control); (*2*) a diagnosis of minimal change disease (MCD), focal segmental glomerulosclerosis (FSGS), membranous nephropathy (MN), or IgA nephropathy; and (*3*) a minimum of two eGFR measurements were included in this study. Participants without recorded outcome event were censored at their last observed eGFR or study visit. Figure 1 shows the sample selection process.

The NEPTUNE Clinical and Demographic Datasets

Demographics, clinical data, disease category, and visually scored pathology data were extracted from the NEPTUNE database.[13] Demographics included age, sex, and race (self-reported or reported by parents of children). Clinical data included eGFR and urine protein creatinine ratio (UPCR) at the time of the biopsy and follow-up data on eGFR and kidney replacement therapy. eGFR was calculated from serum creatinine using the Chronic Kidney Disease Epidemiology Collaboration formula for participants older than 26 years, the modified CKiD-Schwartz formula for participants younger than 18 years, and an average of the two equations for adults age 18–26 years.[14]

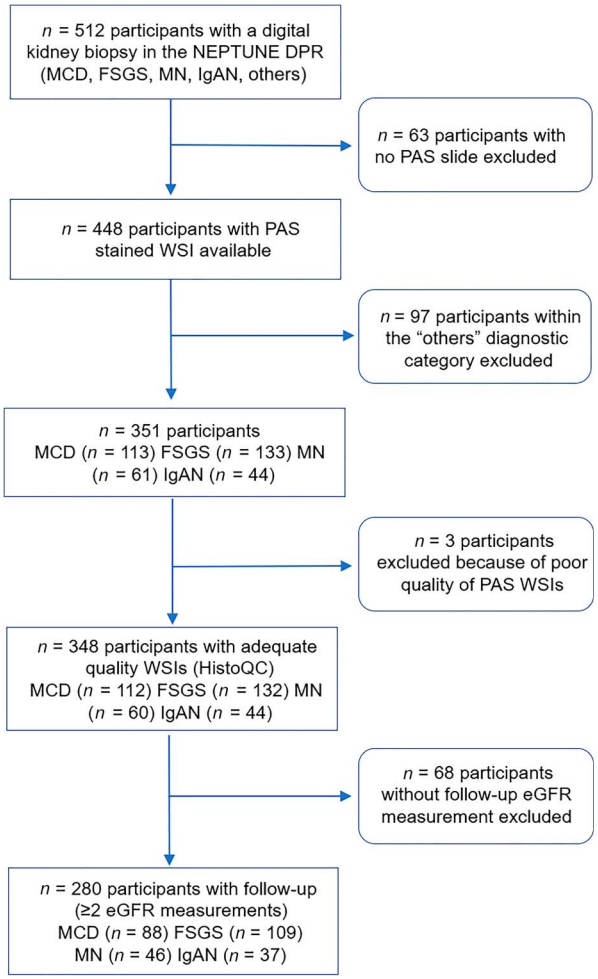

Figure 1. NEPTUNE participants with an adequate quality PAS WSI, a diagnosis of MCD, FSGS, MN, and IgA nephropathy, and adequate clinical data were included in this study. DPR, digital pathology repository.

The clinical outcome of interest was a composite disease progression outcome, defined by time from biopsy to a 40% decline in eGFR, with eGFR <90 ml/min per 1.73 m^2 or kidney failure (dialysis, transplant, or two consecutive eGFRs <15 ml/min per 1.73 m^2).[15]

The NEPTUNE WSI and Pathology Dataset

As part of the NEPTUNE study design, glass slides from formalin-fixed and paraffin-embedded renal biopsies from NEPTUNE participants were scanned into WSIs (Figure 2, first panel, Supplemental Section I). WSIs from glass slides stained with PAS and adequate quality (see WSI quality control) were used in the current study (Figures 1 and 2). Visually scored pathology data included presence of segmental sclerosis (for FSGS, MN, and IgA nephropathy), percentage of acute tubular injury, interstitial inflammation, and interstitial fibrosis.[16,17]

WSI Quality Control

HistoQC,[18] an open-source software designed for quantitative quality control of digital pathology data, was deployed for quality control and data curation (Figure 2, second panel) on 351 PAS WSIs from 351 participants.

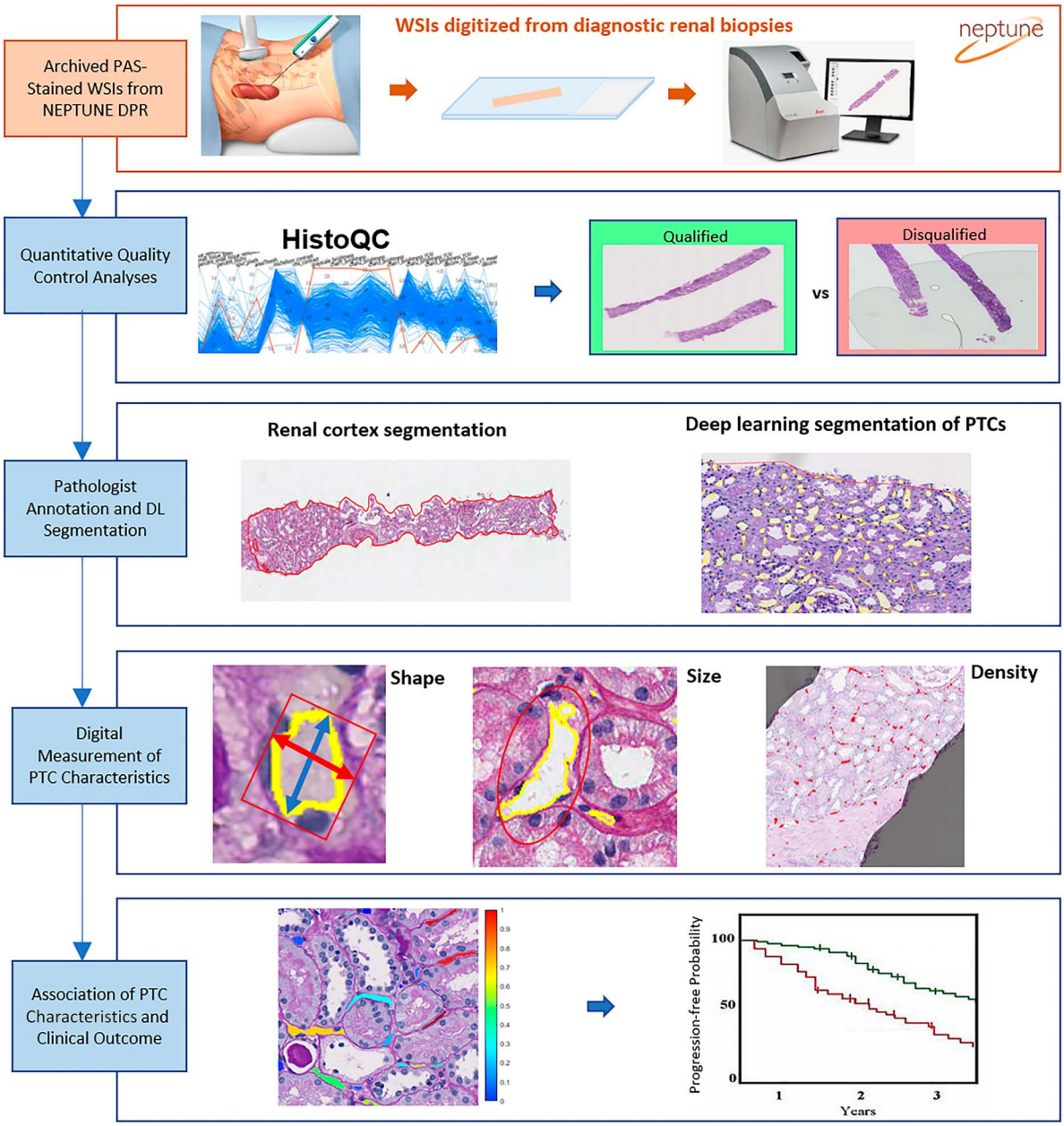

Figure 2. Overview of study design. This study used PAS WSIs from the NEPTUNE DPR (orange box) (top panel). HistoQC was applied to identify and disqualify outlying WSIs with digital pathology artifacts on tissue (*e.g.*, coverslip bubble) (second panel). One qualified WSI per digital biopsy was sent to pathologists for segmentation of the cortex (red outline) (third panel). A previously validated[11] DL segmentation model was used to identify the boundaries of all PTCs within the cortex (yellow outlines) (fourth panel). Quantitative PTC characteristics (shape, size, and density) were then digitally measured from DL-generated PTC segmentations (fifth panel). Finally, Cox proportional hazards models were used to assess the association between PTC characteristics and clinical outcome (bottom panel).

HistoQC was first used to identify WSIs that represented outliers with significant variations in color and intensity characteristics compared with other slides within the cohort. In addition, HistoQC was used to identify artifact-free tissue regions in each WSI. WSIs with artifacts were excluded from downstream analyses[19] (Figure 1).

Quantification of PTC Characteristics

PTC Segmentation

Pathologists manually traced the boundaries of the kidney cortex on each PAS WSI (Figure 2, third panel) using QuPath,[20] an open-source software. Viable cortical PTCs (PTCs with a visible lumen) were segmented using a previously validated deep learning (DL) model[11] (Figure 2, Supplemental Section V). Comparisons of DL PTC segmentation performance with CD34 in interstitial fibrosis and tubular atrophy (IFTA) and non-IFTA regions are shown in Figure 3.

PTC characteristics (shape, density, and size) were computationally measured from the DL-generated PTC segmentations in the cortex (Figure 2, fourth panel, Supplemental Section V).

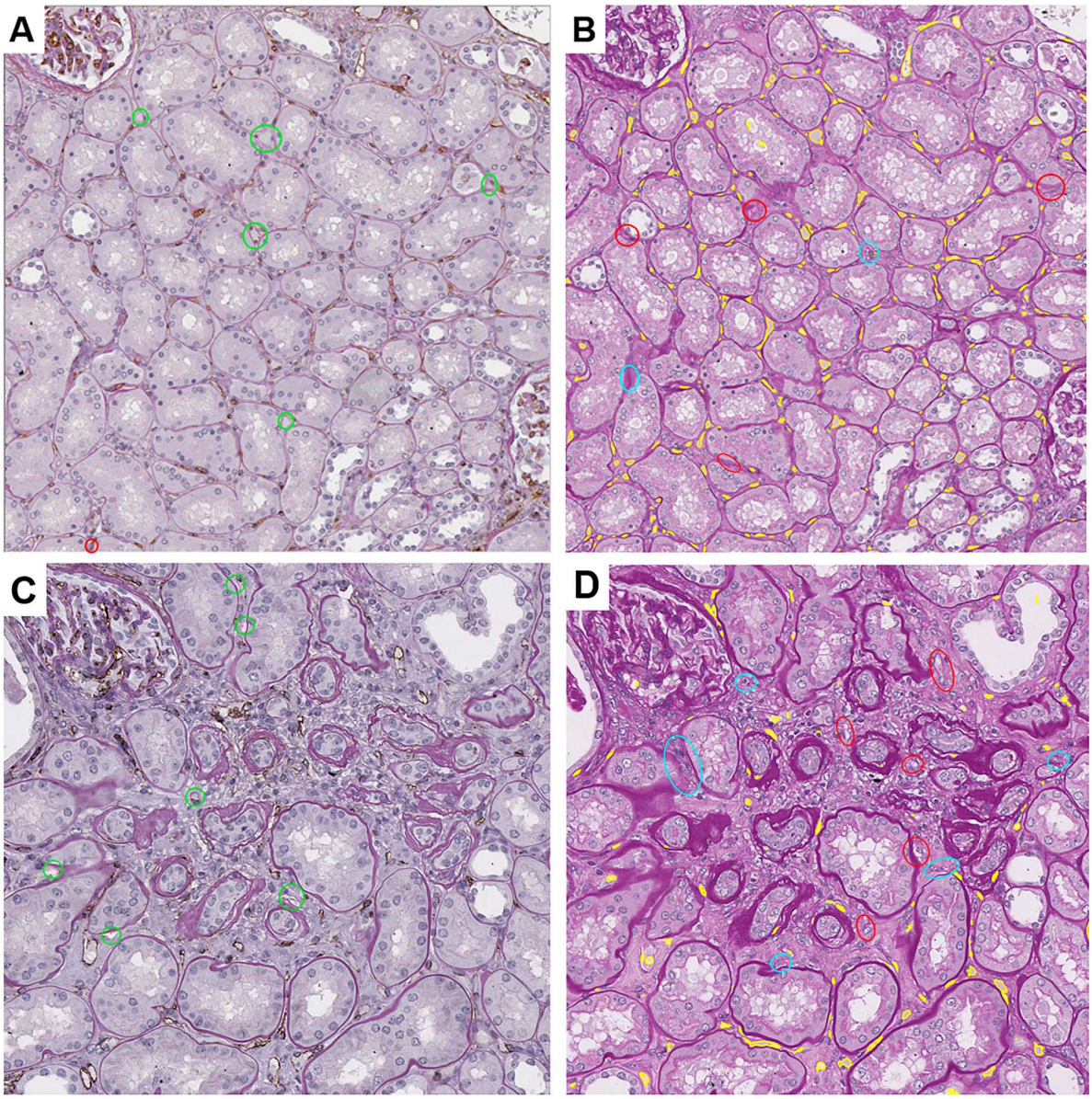

Figure 3. Segmentation outputs of PTCs on PAS nephrectomies. To compare DL segmentation to ground truth defined by immunochemistry, a PAS-stained kidney section from a nephrectomy obtained from the University of Michigan was scanned into a WSI at ×40. The same section was then stained with antibodies against CD34 and rescanned into a WSI at ×40. The immunostaining with antibodies against CD34 highlighted the endothelial cells lining the PTCs in brown. A pathologist visually compared the DL-based PTC segmentations on the PAS and CD34 IHC-stained WSIs. The IHC stain and the DL model detected PTCs with a visible lumen. However, when the PTCs were collapsed, the IHC assay still detected the PTC endothelial cells, but the DL model did not. (A and C) CD34 immunostain over PAS stain in non-IFTA regions (A) and in IFTA regions (C). (B and D) DL PTCs segmentation on PAS (yellow boundaries) in non-IFTA regions (B) and in IFTA regions (D). Only rare PTCs without visible lumens (viable PTCs) were missed by DL model (red circle) in both IFTA (D) and non-IFTA regions (B). Rare PTCs without a visible lumen (nonviable PTCs) were also missed (turquoise circles) (B and D). Rare CD34-negative interstitial spaces with lumen were falsely segmented as PTCs (green circle) (A and C). The IHC stain and the DL model detected PTCs with a visible lumen. However, when the PTCs were collapsed, the IHC assay still detected the PTC endothelial cells, but the DL model did not. Overall, the DL models detected most of the PTCs on PAS-stained images (B and D). IHC, immunohistochemistry.

PTC aspect ratio (shape) was defined as the ratio between the major and the minor axis of the bounding box of a PTC, with larger values denoting more compressed PTCs (Figure 4, left column). The feature quantifies the cross-sectional shape of PTCs. PTC aspect ratios were averaged across all PTCs in the cortex for each biopsy.

PTC density was defined as the ratio between PTC and cortical area measured by the number of pixels (Figure 4, middle column).

PTC size was defined as the cross-sectional area of PTCs in square microns (μm^2), calculated by counting the number of pixels contained within the PTC and multiplying by the size of

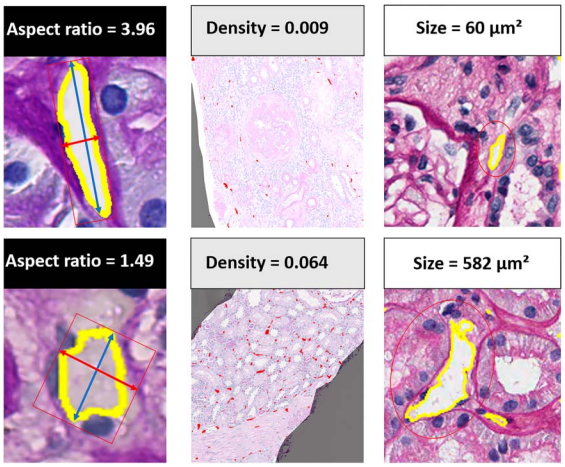

Figure 4. Digital quantification of PTC shape, density, and size from DL segmentations. *Aspect ratio* (left column): PTC boundaries are in yellow and contained within a bounding box (red rectangle). The top image illustrates a PTC with relatively higher aspect ratio (more compressed PTC) and the bottom image a lower aspect ratio. *Density* (middle column): PTCs are in red. Cortical PTC density is low in the top image and high in the lower image. *Size* (right column): PTC boundaries are in yellow. The top image illustrates a small PTC and the bottom image both a large PTC (circled in red) and a small PTC.

each pixel in square microns per pixel. PTC size was averaged across all cortical PTCs in each biopsy (Figure 4, right column).

Relationship Between Quantitative PTC Characteristics and IFTA

IFTA (defined as cortical areas with dense fibrosis and very small tubules with thick tubular basement membranes), was annotated by three pathologists in the cortex for each WSI (Supplemental Figure 9). Quality control of the annotations was performed by the senior pathologist to assure consistency across annotations. The cortical interstitial fractional space was calculated by masking glomeruli and tubules (see Supplemental Section VII). Quantitative PTC characteristics (aspect ratio, density, and size) were computed within and outside cortical IFTA regions. PTC density was also computed within the interstitial fractional space in IFTA and non-IFTA regions.

Statistical Analyses

Descriptive statistics (median and interquartile range for continuous variables and frequency for categorical variables) were used to summarize demographics, clinical characteristics, and computational PTC characteristics. Before subsequent statistical analyses, each of the three PTC characteristics was normalized to a scale of 0–1 by subtracting the minimum value and dividing by the range. Reference examples for normalized PTC characteristics vs. unnormalized are illustrated in Supplemental Section V. Spearman correlation coefficient was used to estimate the correlation between each PTC characteristic and the percentage of interstitial fibrosis from visual assessments (Supplemental Section III). To account for the different follow-up times of study participants and the censoring of patients without recorded event, for each PTC characteristic, an unadjusted Cox proportional hazards model was used to assess the association between the parameter and time to disease progression (Figure 2, bottom panel). To determine the functional form of each association (*i.e.*, whether the association was linear or nonlinear), cubic b-splines and linear splines were used. (additional details are provided in Supplemental Section IV).

For PTC characteristics that were significantly associated with disease progression, multivariable Cox proportional hazards models were used to investigate their independent prognostic value after accounting for other risk factors and known biomarkers of progression. To avoid overfitting because of the limited number of outcome events, a least absolute shrinkage and selection operator (LASSO)-penalized Cox model with five-fold cross-validation for tuning parameter selection was applied first to select adjustment covariates. The LASSO approach was used only to choose relevant adjustment variables to avoid overfitting the multivariable model, whereas the primary exposure of interest (PTC aspect ratio) was forced into the final model without undergoing selection. Potential adjustment covariates included (*1*) demographics, including sex, age, and race (White or Caucasian race versus Black or African American, Asian or Pacific Islander, or multiracial); (*2*) clinical parameters, including disease diagnosis (MCD, FSGS, MN, or IgA nephropathy), UPCR at biopsy, and eGFR at biopsy; (*3*) treatment received by patients, including previous immunosuppression use and previous use of RAAS blockers; and (*4*) other histologic parameters, including the presence of segmental sclerosis, acute tubular injury, interstitial inflammation (percentage of mononuclear white blood cells), and percentage of cortex with interstitial fibrosis. Statistical analyses were conducted using R software, version 4.1.1 (R Development Core Team, Vienna).

Results

Participant Characteristics

After HistoQC-powered quantitative quality control and exclusion of biopsies from participants who did not fit inclusion criteria (Figure 1), N=280 PAS WSIs (one per biopsy) were included: 88 MCD, 109 FSGS, 46 MN, and 37 IgA nephropathy (Table 1). A total of 58 disease progression outcome events were observed. All downstream experimental results were generated on this final cohort of 280 patients.

The distributions of normalized PTC aspect ratio, density, and size across all diseases and within each disease category are illustrated in Supplemental Section II. Across disease diagnoses, all three PTC characteristics were weakly to moderately correlated with interstitial fibrosis (Supplemental Section III).

Association Between PTC Characteristics and Clinical Outcome

PTC Aspect Ratio

A linear spline with one knot at 0.6 was used to model the association between normalized PTC aspect ratio and time to disease progression (Supplemental Section IV). Every 0.1 increase in normalized PTC aspect ratio was associated with 1.28 (1.04 to 1.59) times higher unadjusted hazards of disease progression up to normalized PTC aspect ratio of 0.6 (corresponding to an increase of 5 in unnormalized PTC aspect ratio) (Table 2, $P = 0.019$). Beyond 0.6, we did not find evidence of a significant association between PTC aspect ratio and disease progression. This suggests that more compressed PTCs (higher aspect ratio) are associated with worse patient outcome (Figure 5).

Table 1. Summary of demographics, clinical data at the time of the biopsy, and peritubular capillary characteristics

Variable	Study Sample (*N*=280)
Diagnosis	
MCD	109 (38.9%)
FSGS	88 (31.4%)
MN	46 (16.4%)
IgA nephropathy	37 (13.2%)
Demographics	
Male sex	169 (60.4%)
Age at biopsy, younger than 18 yr	95 (33.9%)
Race	
Asian or Asian American	32 (11.4%)
Black or African American	66 (23.6%)
Others (multiracial or unknown)	31 (11.1%)
White or Caucasian	151 (53.9%)
Baseline laboratory values	
eGFR (ml/min per 1.73 m^2)	81.36 (50.18–106.38)
UPCR (g/g)	5.43 (1.16–7.10)
Computational PTC characteristics	
No. of PTCs segmented	2190 (1335–3297)
PTC aspect ratio	2.94 (2.73–3.20)
Normalized PTC aspect ratio	0.466 (0.333–0.605)
PTC density	1.91% (1.27%–2.77%)
Normalized PTC density	0.180 (0.114–0.266)
PTC size (μm^2)	66.7 (51.3–85.1)
Normalized PTC size	0.229 (0.148–0.311)

Values shown are count (percentage) or median (interquartile range). PTC, peritubular capillary; UPCR, urine protein creatinine ratio; MCD, minimal change disease; FSGS, focal segmental glomerulosclerosis; MN, membranous nephropathy.

The hazard ratio for PTC aspect ratio <0.6 was similar after adjustment (1.28 [1.04–1.59] versus 1.27 [1.01–1.60]) and remained statistically significant (Table 3). Therefore, there was little evidence that the association was confounded by other variables. The association between PTC aspect ratio and disease progression was independent of other factors tested. PTC aspect ratio provides complementary information about the outcome above and beyond that of the known biomarkers, such as interstitial fibrosis and presence of segmental sclerosis.

PTC Density

A linear spline with one knot at 0.4 was used to model the association between normalized PTC density and time to disease progression (Supplemental Section IV). There was little association between PTC density and disease progression up to PTC density of 0.4 ($P = 0.57$, Table 2). Beyond 0.4, every 0.1 increase in density was associated with 35% lower hazards of disease progression, although this association was not statistically significant ($P = 0.36$).

PTC Size

A linear spline with one knot at 0.4 was used to model the association between normalized PTC size and time to disease progression (Supplemental Section IV). There was little association between PTC size and disease progression, both below and above PTC size of 0.4 ($P = 0.72$ and $P = 0.64$, respectively, Table 2).

Quantitative PTC Characteristics in IFTA and Non-IFTA Regions

Although the overall PTC cortical density was higher in IFTA regions compared with non-IFTA regions, when the PTC density was measured in the cortical interstitial fractional space, there was a lower PTC density in IFTA compared with non-IFTA regions (Table 4). Distributions of PTC aspect ratio (Figure 6) or size (Figure 7) were similar between PTCs in IFTA and non-IFTA regions, with the mean IFTA PTC aspect ratio slightly higher and size slightly smaller than those of mean non-IFTA PTC.

Discussion

The limited understanding of the structural and molecular elements that contribute to disease progression is one of the major barriers to effective therapy development and prevention of progression to kidney failure. Several studies have investigated the relationship between structural changes contributing to chronic damage and their association with clinical outcomes.[21–25] There is increasing evidence from studies in animal models that alterations in the interstitial microvasculature, specifically PTC rarefaction, play a major role in the development of interstitial fibrosis and consequently, disease progression,[26–41] and that in in some circumstances, PTC rarefaction could be a better predictor of progression than interstitial fibrosis.[31] These experimental studies elucidated some of the molecular mechanisms that lead to amelioration of renal PTC rarefaction through the use of molecules that target vasodilatation, angiogenesis and repair of the microvasculature, vascular endothelial growth factor (VEGF) signaling,

Table 2. Associations between peritubular capillary characteristics and disease progression

PTC Characteristic	HR (95% CI)	*P* Value
Normalized density <0.4 (per 0.1)	0.92 (0.71 to 1.20)	0.57
Normalized density ≥0.4 (per 0.1)	0.65 (0.26 to 1.62)	0.36
Normalized size <0.4 (per 0.1)	0.95 (0.72 to 1.24)	0.72
Normalized size ≥0.4 (per 0.1)	0.89 (0.55 to 1.44)	0.64
Normalized aspect ratio <0.6 (per 0.1)	1.28 (1.04 to 1.59)	0.019
Normalized aspect ratio ≥0.6 (per 0.1)	0.81 (0.49 to 1.35)	0.43

Unadjusted Cox model results showing estimated associations between peritubular capillary characteristics and time to disease progression (40% eGFR decline or kidney failure) using linear splines with one knot for each peritubular capillary characteristic in separate models. PTC, peritubular capillary; HR, hazard ratio; CI, confidence interval.

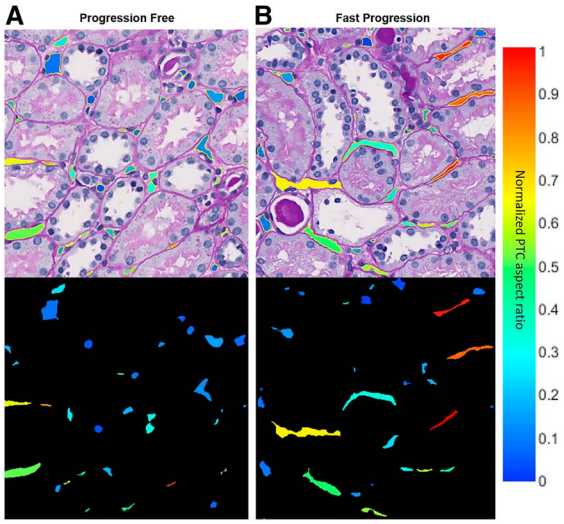

Figure 5. Comparison of representation of PTC aspect ratio in a study participant with good outcome versus one with bad outcome. A heatmap of normalized PTC aspect ratio computed for each PTC is overlaid on top of the PTC segmentation results. (A) Kidney biopsy from a progression-free participant (long follow-up time without disease progression event) compared with (B) a participant with fast progression (short time to disease progression). In the color bar on the right, the scale for normalized PTC aspect ratio values is illustrated—red indicates higher normalized aspect ratio and blue indicates lower normalized aspect ratio. Top row: the heatmap for PTC aspect ratio is overlaid on top of PTC segmentations bounded by yellow outlines. Bottom row: the raw heatmap mapped on the WSIs is illustrated on a dark background for easier visual comparison. The color of PTCs on the heatmap reflects the value of the aspect ratio.

anti-inflammatory and antioxidative pathways, and suppression of endothelial mesenchymal transition.[34,35,37–40,42] The observation that PTC rarefaction is associated with disease progression and age has also been validated in a variety of other human kidney diseases.[26–52,55]

PTC characteristics other than density, such as shape and size, have not yet been extensively studied. As a result, their potential clinical value remains unexplored. Measurement of PTC characteristics has potential applications not only for discovery of mechanisms of disease progression but also in diagnostics. For example, increased PTC size and change in shape (lower aspect ratio) are auxiliary criteria used to assess antibody-mediated rejection in kidney transplant biopsies.[53,54]

Table 3. Adjusted Cox model results showing estimated associations between peritubular capillary aspect ratio and time to disease progression (40% eGFR decline or kidney failure) using adjustment covariates with nonzero coefficients (interstitial fibrosis and segmental sclerosis) from LASSO model

Model	HR (95% CI)	*P* Value
Normalized aspect ratio <0.6 (per 0.1)	1.28 (1.02 to 1.60)	0.031
Normalized aspect ratio ≥0.6 (per 0.1)	0.94 (0.89 to 1.01)	0.11

HR, hazard ratio; CI, confidence interval.

Table 4 Peritubular capillary cortical density controlled by interstitial fibrosis and tubular atrophy and interstitial fractional space

Overall IFTA PTC Cortical Density, %	Overall Non-IFTA PTC Cortical Density outside IFTA, %	IFTA PTC Cortical Density in Interstitial Fractional Space, %	Non-IFTA PTC Density Cortical Density in Interstitial Fractional Space, %
0.75	0.23	1.33	2.57

IFTA, interstitial fibrosis and tubular atrophy; PTC, peritubular capillary.

In spite of overwhelming evidence of PTC involvement in renal diseases, various barriers have previously limited our ability to study PTC characteristics and better understand their role in disease progression. First, methodologies used to detect and quantify PTCs have relied on immunohistochemistry or immunofluorescence using antibodies against endothelial cells (CD34)[28,30,43,51–53] and manual or automated morphometry.[30,43,53] These approaches are expensive, especially if applied to large datasets. In addition, the kidney parenchyma contains a rich microvasculature with large numbers of PTCs, exceeding the ability of visual assessment and thus requiring automation for quantification. Such technology has only recently become feasible. Finally, access to large longitudinal studies with a sufficient number of observations to make meaningful conclusions only recently became available.

Building on these observations[26–55] and leveraging the rich NEPTUNE dataset[13] and powerful image analysis tools,[11,12,21] we extracted selective PTC quantitative features, including density, size, and aspect ratio, from DL-derived PTC segmentations and assessed their associations with disease progression. We demonstrated that the shape of PTCs is a previously unrecognized biomarker of disease progression. Participants with higher PTC aspect ratio values progressed to 40% eGFR decline or kidney failure

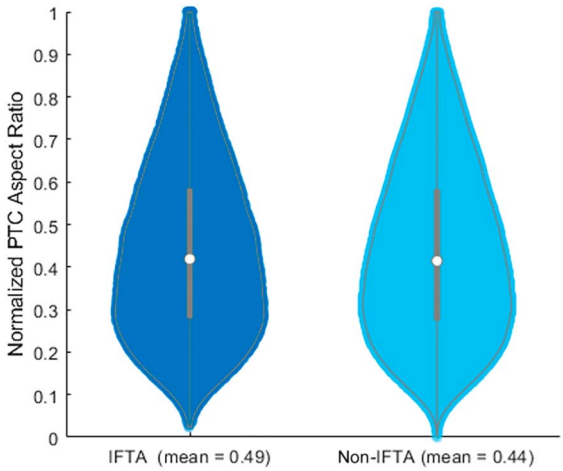

Figure 6. Violin plot showing the distribution of PTC aspect ratio within IFTA (left) versus PTC aspect ratio outside of IFTA (right).

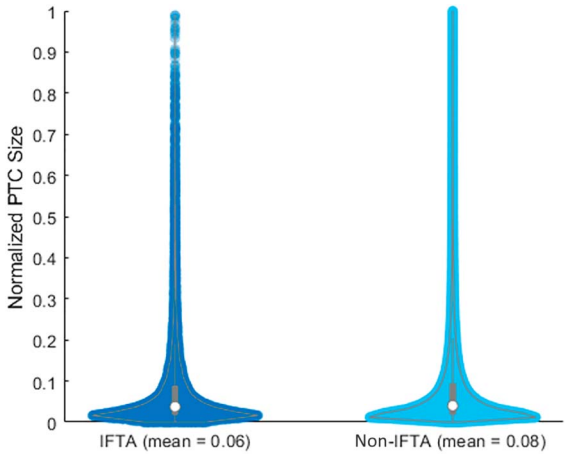

Figure 7. Violin plot showing the distribution of PTC size within IFTA (left) versus PTC size outside of IFTA (right).

significantly faster compared with participants with lower PTC aspect ratio. Two potential reasons might explain this observation. First, a more compressed PTC shape may decrease PTC flow and therefore contribute to the previously mentioned causative relationship between decreased PTC flow and tubulointerstitial scarring.[10] The blood flow and speed in PTCs, in fact, may modulate the exchange of oxygen in the tissue. For example, the cross-section of capillary channels can influence the viscous laminar flow inside the lumen[6–10] while the ratio between the length and the radius of a capillary can modulate the filling rate of a capillary.[8] The causative relationship between PTC flow and tubulointerstitial abnormalities (IFTA) has been previously addressed,[9] demonstrating that the presence of a normal perfusion (normal PTC flow) was associated with a healthy tubulointerstitium while a reduction in PTC flow was associated with tubulointerstitial abnormalities in individuals with idiopathic nephrotic syndrome.[9] In our study, however, the PTC aspect ratio was comparable between IFTA and non-IFTA regions, although there was a weak correlation with interstitial fibrosis scored visually. One potential explanation for the similarity in PTC aspect ratio between the scared and unscarred tubulointerstitium is that our DL model successfully detects viable capillaries (with a visible lumen) but not collapsed/compressed capillaries not contributing to perfusion that are often observed in dense IFTA and detectable only by CD34 stain. We have shown, however, that the number of viable capillaries in IFTA interstitial fractional space was reduced compared with non-IFTA interstitial fractional space. Second, one could speculate that, similar to what has been shown for PTC rarefaction, PTC shape may be modified by morphologic and/or molecular abnormalities at the endothelial cell level,[32,35–38,42,45,55] although this hypothesis would need to be tested in future research.

Although one could argue that the shape of PTCs observed in a 2D section could depend on the angle by which the needle entered the kidney parenchyma, the cortical interstitial microvasculature is formed by a dense net of capillaries running around tubules, with an average of more than 2000 PTCs per cortical tissue biopsy core. It is expected that this large quantity of PTCs should provide sufficient heterogeneity in cross-sectional presentation of the microvasculature within each biopsy to exclude any angle cutting bias.

It is also notable that, although a high aspect ratio largely reflects the more compressed PTC shape, PTCs do not always have a convex shape. As such, a small proportion of PTCs that are flat but bent into a sharp curve can also have a relatively higher aspect ratio.

In line with previous studies,[26,28–32,38,41] we observed a correlation between PTC density and interstitial fibrosis and decreased PTC interstitial fractional space density in IFTA regions compared with non-IFTA regions. However, we did not detect a statistically significant association between overall cortical PTC density and disease progression.

Relatedly, a limitation of our study is the small number of kidney biopsies and outcome events available, although the sample size used in this study remains the largest to date in similar contexts and comprises kidney biopsies obtained and processed in 38 laboratories in North America, suggesting that the biomarker is robust to preanalytical sources of variation.

In summary, we demonstrated the ability to quantitatively measure PTC characteristics in digital kidney biopsies using computational image analysis tools on conventional stains. We also demonstrated the association between PTC shape (aspect ratio) and disease progression in glomerular diseases. Such association appears to be complementary to known biomarkers, including interstitial fibrosis and presence of segmental glomerulosclerosis. We acknowledge that the true power of machine learning is to use hundreds of features, although this approach might lack interpretability. In this study, we focused on a limited set of interpretable features and explored their associations with the status of the tubulointerstitium and clinical outcomes to identify a novel clinical biomarker. Future studies are in progress to validate these observations on independent cohorts of glomerular diseases and chronic and acute kidney diseases and to investigate the topology and spatial relationship between PTCs and other renal functional structures to uncover underlying mechanisms leading to an aberrant cortical microvasculature.

Disclosures

L. Barisoni reports the following: Consultancy: Protalix, Sangamo, and Vertex; Honoraria: Protalix, Sangamo, and Vertex; Advisory or Leadership Role: *Glomerular Disease* Journal, Nature Review Nephrology, and Nephcure Scientific Advisory Board; and Other Interests or Relationships: Nephcure. J.B. Hodgin reports the following: Research Funding: AstraZeneca, Eli Lilly, Gilead, Janssen, Moderna, and Novo Nordisk. L.B. Holzman reports the following: Advisory or Leadership Role: editorial boards for *JASN*, Journal of Clinical Investigation, and Scientific Advisory Board for Nephcure. A.R. Janowczyk reports the following: Consultancy: Lunaphore, Merck, and Roche; and Other Interests or Relationships: Swiss Digital Pathology Consortium. A. Madabhushi reports the following: Consultancy: Aiforia Inc., Biohme Inc., Caris Inc., Roche Inc. Castle Biosciences, and SimBioSys; Ownership Interest: Elucid Bioimaging, Inspirata Inc., and Picture Health; Research Funding: Astrazeneca, Boehringer-Ingelheim, Bristol Myers-Squibb, Eli Lilly, and Philips; Honoraria: Boehringer-Ingelheim and Roche Inc.; Patents or Royalties: Elucid Bioimaging, Inspirata Inc. and Picture Health; and Advisory or Leadership Role: Aiforia Inc, Inspirata, Picture Health, and SimBioSys. L.H. Mariani reports the following:

Consultancy: CKD Advisory Committee, Reata Pharmaceuticals, Travere Therapeutics, Advisory Board; Calliditas Therapeutics, Advisory Board; Chinook Therapeutics, Advisory Board; Research Funding: Boehringer-Ingelheim and Travere Therapeutics; Honoraria: CKD Advisory Committee, Reata Pharmaceuticals, and Travere Therapeutics, Advisory Board; Calliditas Therapeutics, Advisory Board; Chinook Therapeutics, Advisory Board; and Advisory or Leadership Role: Calliditas Therapeutics, Chinook Therapeutics, Reata Pharmaceuticals, and Travere Therapeutics. J. Zee reports the following: Honoraria: Booz Allen Hamilton. All remaining authors have nothing to disclose.

Funding

Research reported in this study was supported by the National Institute of Diabetes and Digestive and Kidney Disease of the National Institutes of Health under the award number 2R01DK118431-04 and the Nephcure foundation.

Research reported in this publication was supported by the National Cancer Institute under award numbers R01CA268287A1, U01CA269181, R01CA26820701A1, R01CA249992-01A1, R01CA202752-01A1, R01CA208236-01A1, R01CA216579-01A1, R01CA220581-01A1, R01CA257612-01A1, 1U01CA239055-01, 1U01CA248226-01, 1U54CA254566-01, National Heart, Lung and Blood Institute 1R01HL15127701A1, R01HL15807101A1, National Institute of Biomedical Imaging and Bioengineering 1R43EB028736-01, VA Merit Review Award IBX004121A from the United States Department of Veterans Affairs Biomedical Laboratory Research and Development Service the Office of the Assistant Secretary of Defense for Health Affairs, through the Breast Cancer Research Program (W81XWH-19-1-0668), the Prostate Cancer Research Program (W81XWH-20-1-0851), the Lung Cancer Research Program (W81XWH-18-1-0440, W81XWH-20-1-0595), the Peer Reviewed Cancer Research Program (W81XWH-18-1-0404, W81XWH-21-1-0345, W81XWH-21-1-0160), and the Kidney Precision Medicine Project (KPMP) Glue Grant and sponsored research agreements from Bristol Myers-Squibb, Boehringer-Ingelheim, Eli-Lilly, and Astrazeneca.

Acknowledgments

The Nephrotic Syndrome Rare Disease Clinical Research Network III (NEPTUNE) is part of the Rare Diseases Clinical Research Network (RDCRN), funded by the National Institutes of Health (NIH) and led by the National Center for Advancing Translational Sciences (NCATS) through its Office of Rare Diseases Research (ORDR). NEPTUNE (U54DK083912) is funded under a collaboration between NCATS and the National Institute of Diabetes and Digestive and Kidney Diseases (NIDDK). Additional funding and/or programmatic support is provided by the University of Michigan, NephCure Kidney International, and the Halpin Foundation. All RDCRN consortia are supported by the RDCRN Data Management and Coordinating Center (DMCC) (U2CTR002818). Funding support for the DMCC is provided by NCATS and the National Institute of Neurological Disorders and Stroke (NINDS).

The content is solely the responsibility of the authors and does not necessarily represent the official views of the National Institutes of Health, the US Department of Veterans Affairs, the Department of Defense, or the US Government.

Author Contributions

Conceptualization: Laura Barisoni, Yijiang Chen, Jeffrey B. Hodgin, Lawrence B. Holzman, Andrew R. Janowczyk, Kyle J. Lafata, Anant Madabhushi, Laura H. Mariani, Jarcy Zee.
Data curation: Laura Barisoni, Yijiang Chen, Jeffrey B. Hodgin, Lawrence B. Holzman, Jeremy Rubin, Paula Toro, Jarcy Zee.
Formal analysis: Laura Barisoni, Yijiang Chen, Jeremy Rubin, Jarcy Zee.
Funding acquisition: Laura Barisoni, Anant Madabhushi.
Investigation: Laura Barisoni, Yijiang Chen, Jeffrey B. Hodgin, Lawrence B. Holzman, Andrew R. Janowczyk, Anant Madabhushi, Jeremy Rubin, Jarcy Zee.
Methodology: Laura Barisoni, Yijiang Chen, Jeffrey B. Hodgin, Lawrence B. Holzman, Andrew R. Janowczyk, Kyle J. Lafata, Anant Madabhushi, Laura H. Mariani, Jarcy Zee.
Project administration: Laura Barisoni, Andrew R. Janowczyk, Anant Madabhushi.
Resources: Laura Barisoni, Anant Madabhushi, Laura H. Mariani.
Software: Yijiang Chen, Jarcy Zee.
Supervision: Laura Barisoni, Andrew R. Janowczyk, Anant Madabhushi, Jarcy Zee.
Validation: Laura Barisoni, Yijiang Chen, Jeremy Rubin.
Visualization: Laura Barisoni, Yijiang Chen.
Writing – original draft: Laura Barisoni, Yijiang Chen, Anant Madabhushi, Jarcy Zee.
Writing – review & editing: Laura Barisoni, Yijiang Chen, Jeffrey B. Hodgin, Lawrence B. Holzman, Andrew R. Janowczyk, Kyle J. Lafata, Anant Madabhushi, Laura H. Mariani, Paula Toro, Jarcy Zee.

Data Sharing Statement

Code availability: The PTC model used in this study is available online here: http://haeckel.case.edu/data/KI_data/; MATLAB code for calculation of PTC quantitative characteristics can be found here: https://github.com/yijiangchen/PTC_quantitative_characteristics.

Supplemental Material

This article contains the following supplemental material online at http://links.lww.com/KN9/A338.

Supplemental Section I. Neptune WSI scanning protocol.

Supplemental Section II. Distribution of quantitative PTC characteristics.

Supplemental Figure 2. Distribution of peritubular capillary (PTC) characteristics summarized by diseases.

Supplemental Section III. Correlation between quantitative PTC characteristics and interstitial fibrosis %.

Supplemental Figure 3. Correlation between the percentage of interstitial fibrosis and PTC characteristics.

Supplemental Figure 4. Correlation between the percentage of interstitial fibrosis and peritubular capillary (PTC) characteristics by disease.

Supplemental Section IV. Assessing the functional form.

Supplemental Figure 5. Unadjusted associations between PTC features and time to disease progression.

Supplemental Section V. Reference examples for normalized PTC characteristics versus unnormalized.

Supplemental Figure 6. Raw versus normalized PTC density.

Supplemental Figure 7. Raw versus normalized PTC size.

Supplemental Figure 8. Raw versus normalized PTC aspect ratio.

Supplemental Section VI. Code availability.

Supplemental Section VII. PTC quantitative characteristics versus IFTA.

Supplemental Figure 9. Pathologist annotation of IFTA (red) on cortex (yellow).

Supplemental Figure 10. Interstitial fractional space.

References

1. Cunningham A, Benediktsson H, Muruve DA, Hildebrand AM, Ravani P. Trends in biopsy-based diagnosis of kidney disease: a population study. *Can J Kidney Health Dis.* 2018;5: 205435811879969. doi:10.1177/2054358118799690
2. Sethi S, Haas M, Markowitz GS, et al. Mayo clinic/renal pathology society consensus report on pathologic classification, diagnosis, and reporting of GN. *J Am Soc Nephrol.* 2016;27(5): 1278–1287. doi:10.1681/ASN.2015060612
3. Mariani LH, Martini S, Barisoni L, et al. Interstitial fibrosis scored on whole-slide digital imaging of kidney biopsies is a predictor of outcome in proteinuric glomerulopathies. *Nephrol Dial Transplant.* 2018;33(2):310–318. doi:10.1093/ndt/gfw443
4. Zhang Y, Jiang Q, Xie J, et al. Modified arteriosclerosis score predicts the outcomes of diabetic kidney disease. *BMC Nephrol.* 2021;22(1):281. doi:10.1186/s12882-021-02492-x
5. Ju W, Nair V, Smith S, et al. Tissue transcriptome-driven identification of epidermal growth factor as a chronic kidney disease biomarker. *Sci Transl Med.* 2015;7(316):316ra193. doi:10.1126/scitranslmed.aac7071
6. Lekner J. Laminar viscous flow through pipes, related to cross-sectional area and perimeter length. *Am J Phys.* 2019;87(10): 791–795. doi:10.1119/1.5113573
7. Akbari M, Sinton D, Bahrami M. Viscous flow in variable cross-section microchannels of arbitrary shapes. *Int J Heat Mass Transfer* 2011;54(17-18):3970–3978. doi:10.1016/j.ijheatmasstransfer.2011.04.028
8. Ridgway CJ, Gane PAC, Schoelkopf J. Effect of capillary element aspect ratio on the dynamic imbibition within porous networks. *J Colloid Interf Sci.* 2002;252(2):373–382. doi:10.1006/jcis.2002.8468
9. Futrakul N, Yenrudi S, Sensirivatana R, et al. Peritubular capillary flow determines tubulointerstitial disease in idiopathic nephrotic syndrome. *Ren Fail.* 2000;22(3):329–335. doi:10.1081/jdi-100100876
10. Wu B. The influence of the cross section shape on channel flow: modeling, simulation and experiment. Modeling and Simulation. Université de Grenoble, 2014. English. (NNT). Available at https://theses.hal.science/tel-00938250v1
11. Jayapandian CP, Chen Y, Janowczyk AR, et al. Development and evaluation of deep learning–based segmentation of histologic structures in the kidney cortex with multiple histologic stains. *Kidney Int.* 2021;99(1):86–101. doi:10.1016/j.kint.2020.07.044
12. Madabhushi A, Lee G. Image analysis and machine learning in digital pathology: challenges and opportunities. *Med Image Anal.* 2016;33:170–175. doi:10.1016/j.media.2016.06.037
13. Gadegbeku CA, Gipson DS, Holzman LB, et al. Design of the Nephrotic Syndrome Study Network (NEPTUNE) to evaluate primary glomerular nephropathy by a multidisciplinary approach. *Kidney Int.* 2013;83(4):749–756. doi:10.1038/ki.2012.428
14. Ng DK, Schwartz GJ, Schneider MF, Furth SL, Warady BA. Combination of pediatric and adult formulas yield valid glomerular filtration rate estimates in young adults with a history of pediatric chronic kidney disease. *Kidney Int.* 2018;94(1): 170–177. doi:10.1016/j.kint.2018.01.034
15. Zee J, Mansfield S, Mariani LH, Gillespie BW. Using all longitudinal data to define time to specified percentages of estimated GFR decline: a simulation study. *Am J Kidney Dis.* 2019;73(1): 82–89. doi:10.1053/j.ajkd.2018.07.009
16. Barisoni L, Nast CC, Jennette JC, et al. Digital pathology evaluation in the multicenter Nephrotic Syndrome Study Network (NEPTUNE). *Clin J Am Soc Nephrol.* 2013;8(8):1449–1459. doi:10.2215/CJN.08370812
17. Nast CC, Lemley KV, Hodgin JB, et al. Morphology in the digital age: integrating high-resolution description of structural alterations with phenotypes and genotypes. *Semin Nephrol.* 2015; 35(3):266–278. doi:10.1016/j.semnephrol.2015.04.006
18. Janowczyk A, Zuo R, Gilmore H, Feldman M, Madabhushi A. HistoQC: an open-source quality control tool for digital pathology slides. *JCO Clin Cancer Inform.* 2019;3:1–7. doi:10.1200/CCI.18.00157
19. Chen Y, Zee J, Smith A, et al. Assessment of a computerized quantitative quality control tool for whole slide images of kidney biopsies. *J Pathol.* 2021;253(3):268–278. doi:10.1002/path.5590
20. Bankhead P, Loughrey MB, Fernández JA, et al. QuPath: open source software for digital pathology image analysis. *Sci Rep.* 2017;7(1):16878. doi:10.1038/s41598-017-17204-5
21. Barisoni L, Lafata KJ, Hewitt SM, Madabhushi A, Balis UGJ. Digital pathology and computational image analysis in nephropathology. *Nat Rev Nephrol.* 2020;16(11):669–685. doi:10.1038/s41581-020-0321-6
22. Jacobs-Cachá C, Vergara A, García-Carro C, et al. Challenges in primary focal segmental glomerulosclerosis diagnosis: from the diagnostic algorithm to novel biomarkers. *Clin Kidney J.* 2021; 14(2):482–491. doi:10.1093/ckj/sfaa110
23. Hodgin JB, Mariani LH, Zee J, et al. Quantification of glomerular structural lesions: associations with clinical outcomes and transcriptomic profiles in nephrotic syndrome. *Am J Kidney Dis.* 2022;79(6):807–819.e1. doi:10.1053/j.ajkd.2021.10.004
24. Cook HT, Cattran DC, Coppo R, et al. The Oxford classification of IgA nephropathy: rationale, clinicopathological correlations, and classification. *Kidney Int.* 2009;76(5):534–545. doi:10.1038/ki.2009.243
25. Roberts IS, Troyanov S, Cook HT, et al. The Oxford classification of IgA nephropathy: pathology definitions, correlations, and reproducibility. *Kidney Int.* 2009;76(5):546–556. doi:10.1038/ki.2009.168
26. Lindenmeyer MT, Kretzler M, Boucherot A, et al. Interstitial vascular rarefaction and reduced VEGF-A expression in human diabetic nephropathy. *J Am Soc Nephrol.* 2007;18(6): 1765–1776. doi:10.1681/ASN.2006121304
27. Kramann R, Tanaka M, Humphreys BD. Fluorescence microangiography for quantitative assessment of peritubular capillary changes after AKI in mice. *J Am Soc Nephrol.* 2014;25(9): 1924–1931. doi:10.1681/ASN.2013101121
28. Kida Y. Peritubular capillary rarefaction: an underappreciated regulator of CKD progression. *Int J Mol Sci.* 2020;21(21):8255. doi:10.3390/ijms21218255
29. Namikoshi T, Satoh M, Horike H, et al. Implication of peritubular capillary loss and altered expression of vascular endothelial growth factor in IgA nephropathy. *Nephron Physiol.* 2006;102(1): p9–p16. doi:10.1159/000088405
30. Choi YJ, Chakraborty S, Nguyen V, et al. Peritubular capillary loss is associated with chronic tubulointerstitial injury in human kidney: altered expression of vascular endothelial growth factor. *Hum Pathol.* 2000;31(12):1491–1497. doi:10.1053/hupa.2000.20373
31. Menshikh A, Scarfe L, Delgado R, et al. Capillary rarefaction is more closely associated with CKD progression after cisplatin, rhabdomyolysis, and ischemia-reperfusion-induced AKI than renal fibrosis. *Am J Physiol Renal Physiol.* 2019;317(5): F1383–F1397. doi:10.1152/ajprenal.00366.2019
32. Bábíčková J, Klinkhammer BM, Buhl EM, et al. Regardless of etiology, progressive renal disease causes ultrastructural and functional alterations of peritubular capillaries. *Kidney Int.* 2017; 91(1):70–85. doi:10.1016/j.kint.2016.07.038
33. Liu TT, Luo R, Yang Y, et al. LRG1 mitigates renal interstitial fibrosis through alleviating capillary rarefaction and inhibiting inflammatory and pro-fibrotic cytokines. *Am J Nephrol.* 2021; 52(3):228–238. doi:10.1159/000514167
34. Ferguson CM, Farahani RA, Zhu XY, et al. Mesenchymal stem/stromal cell-derived extracellular vesicles elicit better preservation of the intra-renal microvasculature than renal revascularization in pigs with renovascular disease. *Cells* 2021; 10(4):763. doi:10.3390/cells10040763
35. Wang Y, Zuo B, Wang N, Li S, Liu C, Sun D. Calcium dobesilate mediates renal interstitial fibrosis and delay renal peritubular capillary loss through Sirt1/p53 signaling pathway. *Biomed Pharmacother.* 2020;132:110798. doi:10.1016/j.biopha.2020.110798
36. Cui J, Wu X, Song Y, Chen Y, Wan J. Complement C3 exacerbates renal interstitial fibrosis by facilitating the M1 macrophage phenotype in a mouse model of unilateral ureteral obstruction. *Am J Physiol Renal Physiol.* 2019;317(5):F1171–F1182. doi:10.1152/ajprenal.00165.2019
37. Zhao J, Meng M, Zhang J, et al. Astaxanthin ameliorates renal interstitial fibrosis and peritubular capillary rarefaction in unilateral ureteral obstruction. *Mol Med Rep.* 2019;19(4): 3168–3178. doi:10.3892/mmr.2019.9970
38. Choi HY, Lee HG, Kim BS, et al. Mesenchymal stem cell-derived microparticles ameliorate peritubular capillary

rarefaction via inhibition of endothelial-mesenchymal transition and decrease tubulointerstitial fibrosis in unilateral ureteral obstruction. *Stem Cell Res Ther.* 2015;6(1):18. doi:10.1186/s13287-015-0012-6
39. Li S, Wang Y, Chen L, et al. Beraprost sodium mitigates renal interstitial fibrosis through repairing renal microvessels. *J Mol Med.* 2019;97(6):777–791. doi:10.1007/s00109-019-01769-x
40. Zsengellér ZK, Lo A, Tavasoli M, Pernicone E, Karumanchi SA, Rosen S. Soluble fms-like tyrosine kinase 1 localization in renal biopsies of CKD. *Kidney Int Rep.* 2019;4(12):1735–1741. doi:10.1016/j.ekir.2019.08.004
41. Kramann R, Humphreys BD. Kidney pericytes: roles in regeneration and fibrosis. *Semin Nephrol.* 2014;34(4):374–383. doi:10.1016/j.semnephrol.2014.06.004
42. O'Brien K, Saravanabavan S, Zhang JQJ, et al. Regression of peritubular capillaries coincides with angiogenesis and renal cyst growth in experimental polycystic kidney disease. *Int J Nephrol Renovasc Dis.* 2020;13:53–64. doi:10.2147/IJNRD.S238767
43. Zhang J, Cong J, Yang J, et al. Morphologic and morphometric study on microvasculature of developing mouse kidneys. *Am J Physiol Renal Physiol.* 2018;315(4):F852–F860. doi:10.1152/ajprenal.00615.2017
44. Sean Eardley K, Cockwell P. Macrophages and progressive tubulointerstitial disease. *Kidney Int.* 2005;68(2):437–455. doi:10.1111/j.1523-1755.2005.00422.x
45. Kaukinen A, Lautenschlager I, Helin H, Karikoski R, Jalanko H. Peritubular capillaries are rarefied in congenital nephrotic syndrome of the Finnish type. *Kidney Int.* 2009;75(10):1099–1108. doi:10.1038/ki.2009.41
46. Doreille A, Azzi F, Larivière-Beaudoin S, et al. Acute kidney injury, microvascular rarefaction, and estimated glomerular filtration rate in kidney transplant recipients. *Clin J Am Soc Nephrol.* 2021;16(3):415–426. doi:10.2215/CJN.07270520
47. Lombardi D, Gordon KL, Polinsky P, Suga S, Schwartz SM, Johnson RJ. Salt-sensitive hypertension develops after short-term exposure to angiotensin II. *Hypertension.* 1999;33(4):1013–1019. doi:10.1161/01.HYP.33.4.1013
48. Iwazu Y, Muto S, Fujisawa G, et al. Spironolactone suppresses peritubular capillary loss and prevents deoxycorticosterone acetate/salt-induced tubulointerstitial fibrosis. *Hypertension.* 2008;51(3):749–754. doi:10.1161/HYPERTENSIONAHA.107.104901
49. Anutrakulchai S, Titipungul T, Pattay T, et al. Relation of peritubular capillary features to class of lupus nephritis. *BMC Nephrol.* 2016;17(1):169. doi:10.1186/s12882-016-0388-2
50. Wei W, Popov V, Walocha JA, Wen J, Bello-Reuss E. Evidence of angiogenesis and microvascular regression in autosomal-dominant polycystic kidney disease kidneys: a corrosion cast study. *Kidney Int.* 2006;70(7):1261–1268. doi:10.1038/sj.ki.5001725
51. Ishii Y, Sawada T, Kubota K, Fuchinoue S, Teraoka S, Shimizu A. Injury and progressive loss of peritubular capillaries in the development of chronic allograft nephropathy. *Kidney Int.* 2005;67(1):321–332. doi:10.1111/j.1523-1755.2005.00085.x
52. Koller GM, Schafer C, Kemp SS, et al. Proinflammatory mediators, IL (Interleukin)-1β, TNF (tumor necrosis factor) α, and thrombin directly induce capillary tube regression. *Arterioscler Thromb Vasc Biol.* 2020;40(2):365–377. doi:10.1161/ATVBAHA.119.313536
53. Li X, Sun Q, Zhang M, Xie K, Chen J, Liu Z. Capillary dilation and rarefaction are correlated with intracapillary inflammation in antibody-mediated rejection. *J Immunol Res.* 2014;2014:1–10. doi:10.1155/2014/582902
54. Roufosse C, Simmonds N, Clahsen-van Groningen M, et al. A 2018 reference guide to the banff classification of renal allograft pathology. *Transplantation.* 2018;102(11):1795–1814. doi:10.1097/TP.0000000000002366
55. Dinda A, Singh K, Ray R, Sharma A, Gupta R, Bagga A. Peritubular capillaries and renal function in pediatric idiopathic nephrotic syndrome. *Saudi J Kidney Dis Transpl.* 2013;24(5):942–949. doi:10.4103/1319-2442.118091

Received: June 14, 2022 **Accepted:** February 13, 2023
Published Online Ahead of Print: April 5, 2023

Yijiang Chen and Jarcy Zee contributed equally to this work.

See related editorial, "Machine Learning Illuminates the Extraglomerular Microvasculature," on pages 578–579.